

## Article

# Defect-free Phononic Crystal Waveguides on GaAs: Supplemental Information

Edward Muzar <sup>1</sup> and James A. H. Stotz <sup>1,\*</sup> 

<sup>1</sup> Department of Physics, Engineering Physics & Astronomy, Queen's University, Kingston, ON K7L 3N6, Canada

\* Correspondence: jstotz@queensu.ca

**Abstract:** This Supplemental Information contains three sections supporting the work presented in the main article. Section S1 provides additional information surrounding the methods used when modelling in COMSOL. Section S2 provides a number of simulations that adjust the boundary conditions and mesh geometries with little impact on the results. Finally, Section S3 displays simulation data consisting of the the total displacement fields for the phononic crystal waveguides with crystal widths ranging from 1 to 12 holes.

**Keywords:** Phononic Crystal; Waveguide; Gallium Arsenide; Finite Element

## S1. Materials and Methods: Additional Information

As discussed in the main text, modelling was performed using the finite element method (FEM) in a fully three-dimensional geometry using COMSOL Multiphysics, version 5, along with the Solid Mechanics and MEMS modules. However, either of the Acoustics or MEMS modules is sufficient to provide piezoelectric response. Choice was determined by COMSOL, which also considered the availability of the shared license. For validation of the FEM model presented here, only the Solid Mechanics modules was used. For the structural mechanics modelling presented, COMSOL performs an eigenfrequency analysis, using the PARDISO eigenvalue direct solver for this work, of the system's matrix equation of motion:[1]

$$\left(-\omega^2 \mathbf{M} + i\omega \mathbf{C} + \mathbf{K}\right) \tilde{\mathbf{u}} e^{i\omega t} = 0 \quad (1)$$

In addition to Bloch-Floquet periodic and tractionless boundary conditions, the COMSOL's built-in Low-Reflecting boundary condition was used in the simulations and is governed by the equation[1,2]

$$\mathbf{T} \cdot \mathbf{n} = i\omega [\rho v_L (\mathbf{u} \cdot \mathbf{n}) \mathbf{n} + \rho v_S (\mathbf{u} \cdot \mathbf{t}) \mathbf{t}], \quad (2)$$

which is presented in its frequency-domain formulation for eigenfrequency analysis. In Eqn. 2,  $\mathbf{n}$  and  $\mathbf{t}$  are the unit normal and tangential vectors at the boundary,  $\mathbf{T}$  is the stress tensor,  $\rho$  is the density,  $\omega$  is the frequency, and  $v_L$  and  $v_S$  are the longitudinal and shear phase velocities, respectively. The values for  $v_L$  and  $v_S$  were default values from the COMSOL Material Library.

## S2. Additional Simulation Parameters

### S2.1 Low-Reflecting Boundary Condition

The Low-Reflecting (LR) boundary conditions in COMSOL described above provide near perfectly absorbing boundaries without the extra computational volume required for boundary conditions implementing a perfectly matched layer (PML). As an example, the 4-inclusion wide geometry (with a cladding of eight lattice parameters ( $8a$ ) or  $40 \mu\text{m}$ )

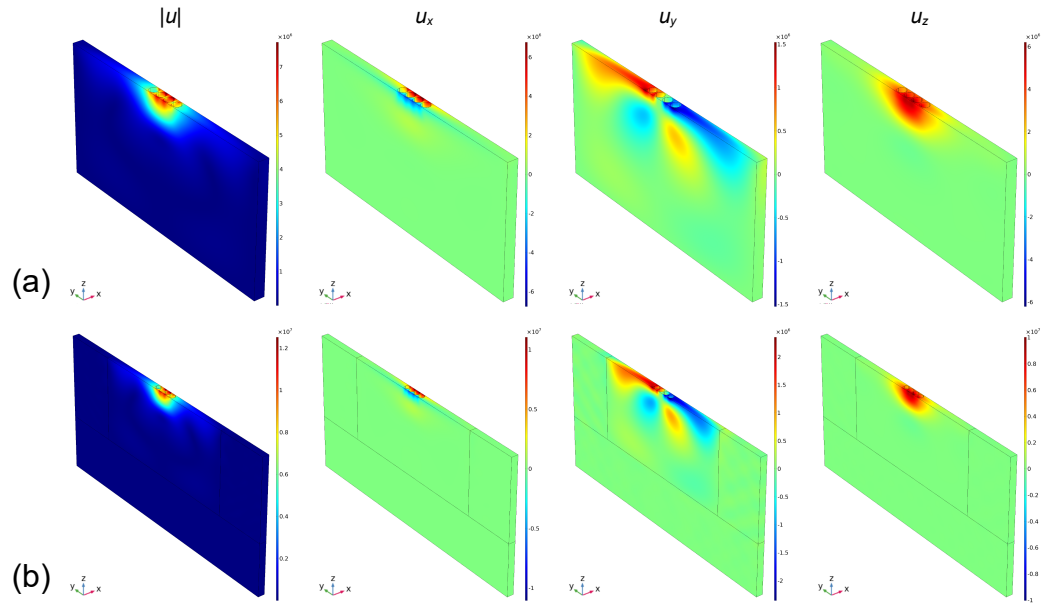


**Figure 1.** The magnitude of the total displacement field  $|u|$  as well as the  $x$ -,  $y$ -, and  $z$ -component fields for the 4-inclusion wide waveguide. The computational domain within the boundaries is  $4\ \mu\text{m}$ ,  $96\ \mu\text{m}$ , and  $50\ \mu\text{m}$  in the  $x$ -,  $y$ -, and  $z$ -directions, respectively. The upper panels in (a) correspond to the simulation using the Low-Reflecting boundaries along the  $y$ -planes while the lower (b) panels use COMSOL's perfectly matched layer (PML) boundaries using a PML Scaling Factor of 1 and extending  $32\ \mu\text{m}$  (8a) from the domain. The real frequencies of the eigenmodes are  $175.30\ \text{MHz}$  for (a) and  $175.28\ \text{MHz}$  for (b).

was modelled using both the Low-Reflecting boundary and the PML boundary (with extents of  $32\ \mu\text{m}$ ) as shown in Fig. 1(a) and Fig. 1(b), respectively. The features in both types of boundary conditions are near identical, and the real frequencies of the modes are  $175.30\ \text{MHz}$  (LR) and  $175.28\ \text{MHz}$  (PML), which are near identical and only slightly different from the  $175.40\ \text{MHz}$  quoted in the main article and arises from small computational variances. The quality of the Low-Reflecting boundary stems from the fact that there is little acoustic energy stretching to the  $y$ -boundary, and the component that does is the  $y$ -displacement field. This component advancing normal to the boundary is near optimal for the LR boundary condition.

### S2.2 Modelling Independence of Geometry

The computational volume was meshed using COMSOL, and in the main article, used a maximum mesh element size of  $a/4$  or  $1\ \mu\text{m}$  and a minimum mesh element size of  $a/40$  or  $0.1\ \mu\text{m}$ . To generate different mesh configurations, simulations were performed for maximum mesh element sizes of  $a/3$  and  $a/5$  (Figs. 2(a) and (c)) in addition to simulations where both the minimum and maximum mesh sizes were fixed to  $a/4$  and  $a/5$  for Figs. 2(d) and (e), respectively. For these simulations, a slightly smaller computational width of  $72\ \mu\text{m}$  was chosen (or  $28\ \mu\text{m}$  of cladding (7a) on either side of the waveguide), and LR lateral boundary conditions were used. Comparing the different geometries, the displacement fields display consistent features not only across the different meshing, but also with the geometries with periodic boundary conditions below (Figs. 3 to 14) and with the larger computational domain in the main article. Further more, the real frequencies of the eigenmodes in Figs. 2(a) through (c) ( $175.49\ \text{MHz}$  ( $a/3$ ),  $175.46\ \text{MHz}$  ( $a/4$ ), and  $175.45\ \text{MHz}$  ( $a/5$ )) are consistent with other values for the 4-inclusion waveguide and show an independence across the many computational configurations presented. For the larger meshes of Figs. 2(d) and (e), there is a slight increase in the real frequency from of the mode

from all other mesh configurations as the mesh size increases from  $a/5$  (175.59 MHz) to

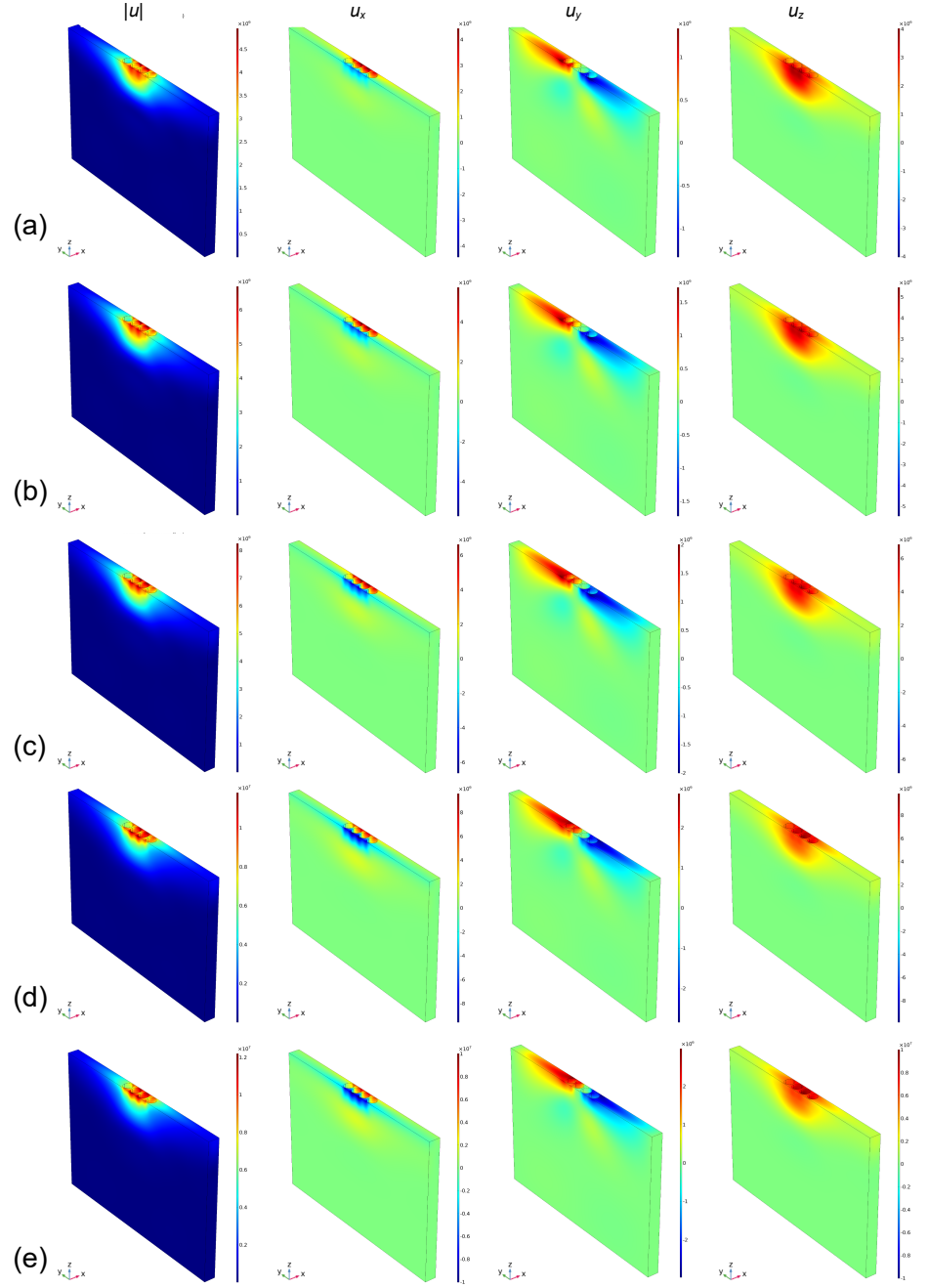


**Figure 2.** The magnitude of the total displacement field as well as the  $x$ -,  $y$ -, and  $z$ -component fields for the 4-inclusion wide waveguide. The differences shown correspond to different maximum mesh element sizes being: (a)  $a/3$  (b)  $a/4$ , and (c)  $a/5$ . The minimum mesh size for (a) through (c) is  $a/40$ . Coarser meshes are shown in (d) and (e), where both the minimum and maximum mesh sizes are specified as  $a/4$  and  $a/5$ , respectively. Low-Reflecting boundaries were used along the  $y$ -planes for all simulations. The real frequencies of the eigenmodes for the associate displacement maps are: (a) 175.49 MHz, (b) 175.46 MHz, (c) 175.45 MHz, (d) 175.70 MHz, and (e) 175.59 MHz. The computational domain for all simulations is  $4 \mu\text{m}$ ,  $72 \mu\text{m}$ , and  $50 \mu\text{m}$  in the  $x$ -,  $y$ -, and  $z$ -directions, respectively.

### S3. Additional Simulation Results

Figures 3 through 14 contains plots of the simulation data for the total displacement magnitudes for waveguides from 1 to 12 holes wide, respectively. The computational domain for these simulations is  $4\ \mu\text{m}$  and  $50\ \mu\text{m}$  in the  $x$ -, and  $z$ -directions, respectively. In the  $y$ -direction, the domain size is allowed to increase in size to maintain the cladding (bare surface) sizes outside of the waveguide at  $28\ \mu\text{m}$  on either side, or  $7a$  wide. As mentioned in the main text, periodic boundary conditions are used at the end of the cladding ( $y$ -extents) that result in an infinite number of adjacent waveguides being simulated. The real part of the eigenfrequency for each mode is provided in each caption, and each mode is the lowest frequency (Rayleigh) mode for each configuration. It is interesting to note that when even when using periodic boundary conditions, the eigenfrequency of the four-inclusion waveguide ( $175.43\ \text{MHz}$ ) remains consistent with the other computational geometries.

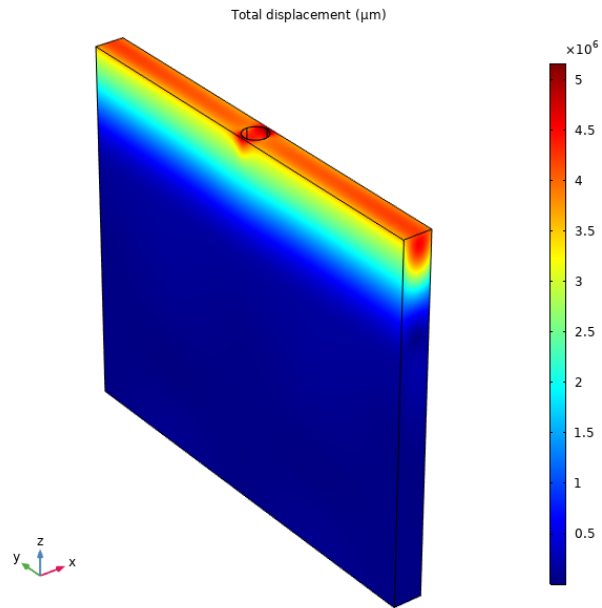


**Figure 3.** The magnitude of the total displacement field from the mode for the one-inclusion waveguide consisting of a single  $3\ \mu\text{m}$  deep inclusion. The eigenfrequency that was determined and displayed is  $177.87\ \text{MHz}$ .

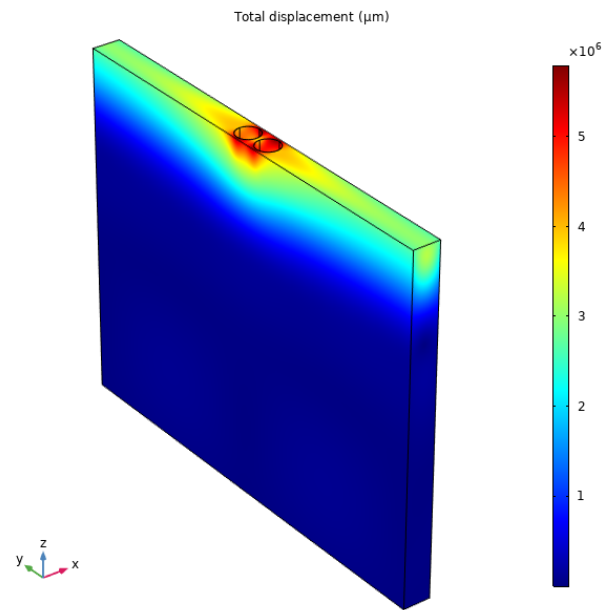


**Figure 4.** The magnitude of the total displacement field from the mode for the two-inclusion waveguide consisting of two  $3\ \mu\text{m}$  deep inclusions. The eigenfrequency that was determined and displayed is 177.43 MHz.

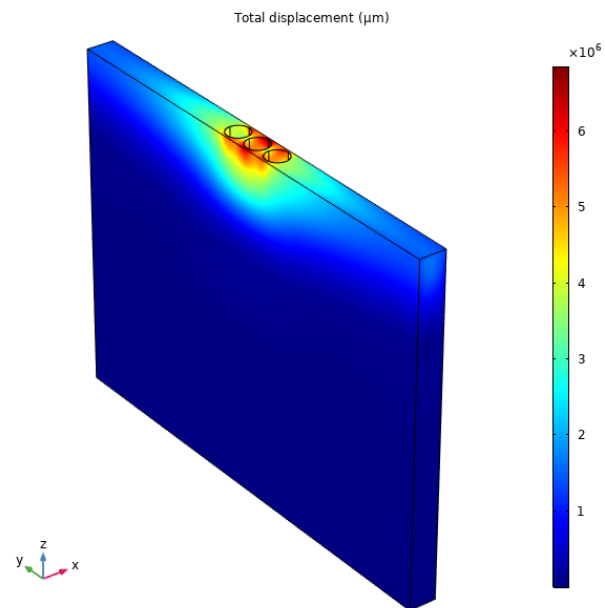


**Figure 5.** The magnitude of the total displacement field from the mode for the three-inclusion waveguide consisting of three  $3\ \mu\text{m}$  deep inclusions. The eigenfrequency that was determined and displayed is 173.36 MHz.

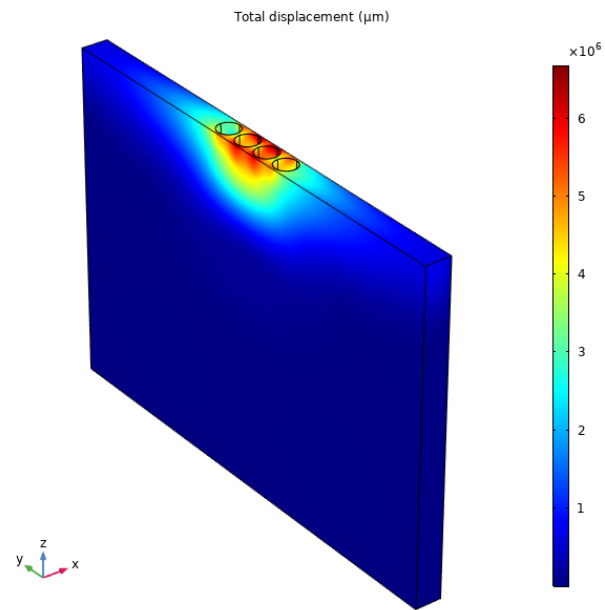


**Figure 6.** The magnitude of the total displacement field from the mode for the four-inclusion waveguide consisting of four  $3\ \mu\text{m}$  deep inclusions. The eigenfrequency that was determined and displayed is 175.43 MHz.

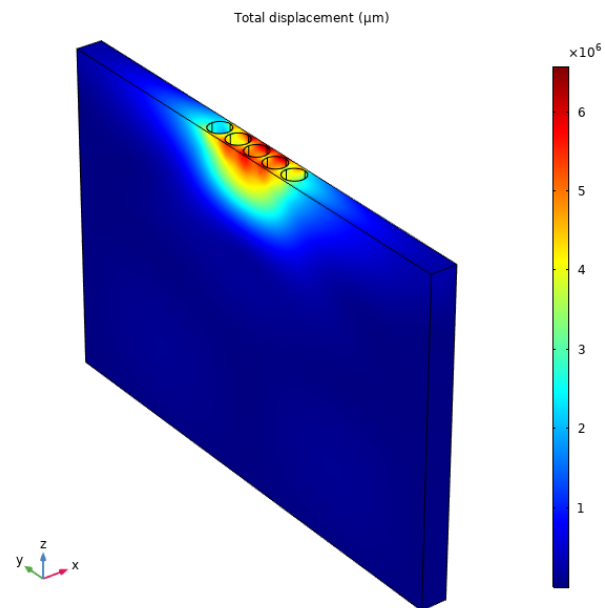


**Figure 7.** The magnitude of the total displacement field from the mode for the five-inclusion waveguide consisting of five  $3\ \mu\text{m}$  deep inclusions. The eigenfrequency that was determined and displayed is 174.32 MHz.

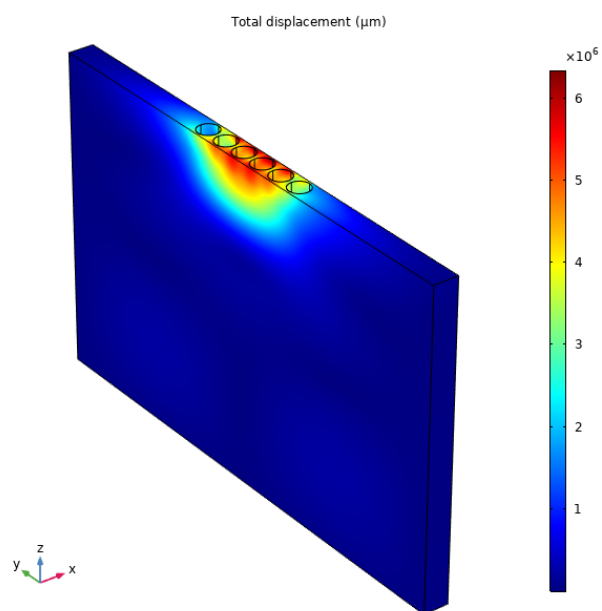


**Figure 8.** The magnitude of the total displacement field from the mode for the six-inclusion waveguide consisting of six  $3\ \mu\text{m}$  deep inclusions. The eigenfrequency that was determined and displayed is 173.36 MHz.

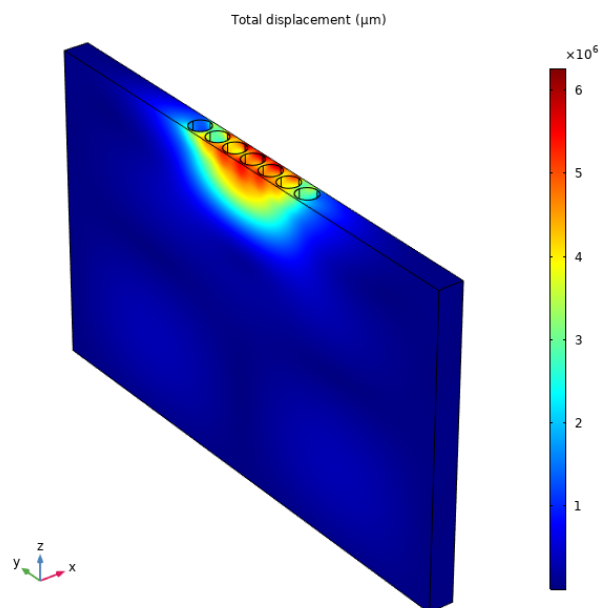


**Figure 9.** The magnitude of the total displacement field from the mode for the seven-inclusion waveguide consisting of seven  $3\ \mu\text{m}$  deep inclusions. The eigenfrequency that was determined and displayed is 172.6 MHz.

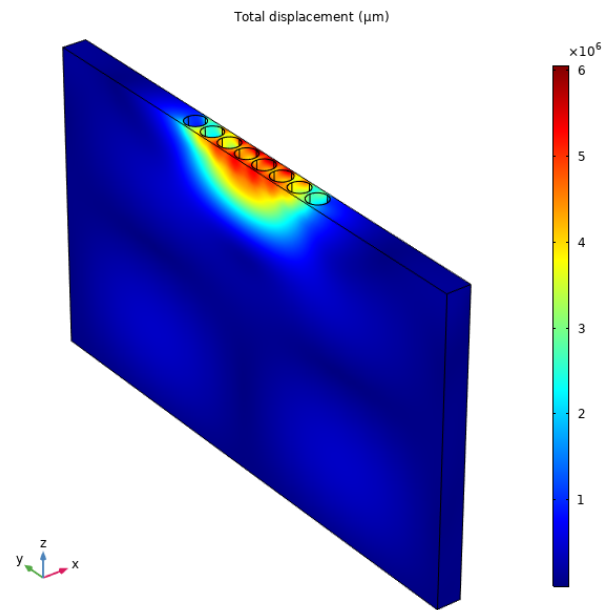


**Figure 10.** The magnitude of the total displacement field from the mode for the eight-inclusion waveguide consisting of eight  $3\ \mu\text{m}$  deep inclusions. The eigenfrequency that was determined and displayed is 172.01 MHz.

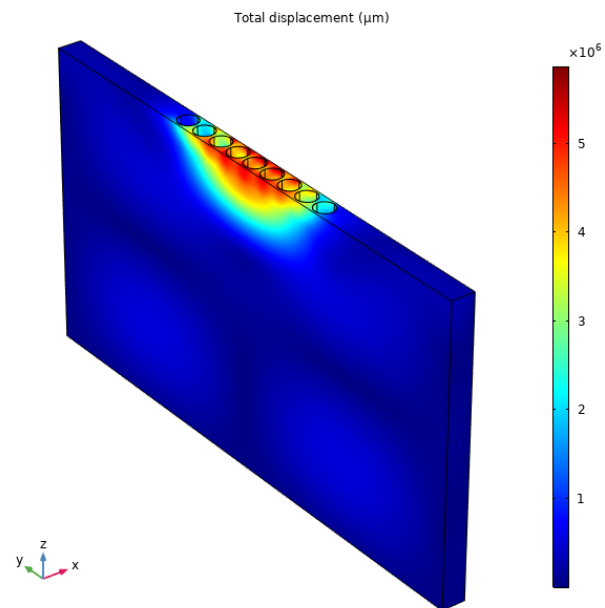


**Figure 11.** The magnitude of the total displacement field from the mode for the nine-inclusion waveguide consisting of nine  $3\ \mu\text{m}$  deep inclusions. The eigenfrequency that was determined and displayed is 171.52 MHz.



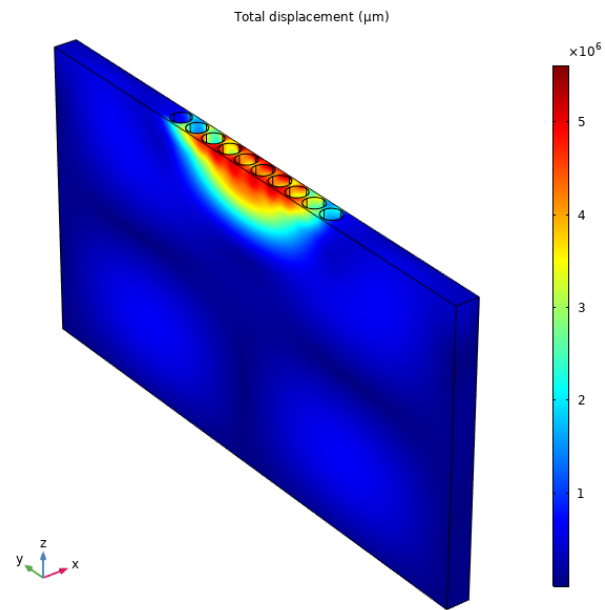


**Figure 12.** The magnitude of the total displacement field from the mode for the ten-inclusion waveguide consisting of ten  $3\text{ }\mu\text{m}$  deep inclusions. The eigenfrequency that was determined and displayed is 171.01 MHz.

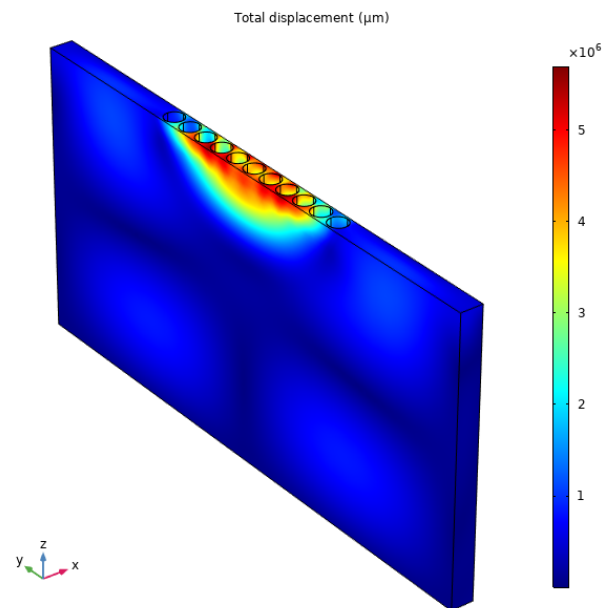


**Figure 13.** The magnitude of the total displacement field from the mode for eleven two-inclusion waveguide consisting of eleven  $3\text{ }\mu\text{m}$  deep inclusions. The eigenfrequency that was determined and displayed is 170.63 MHz.

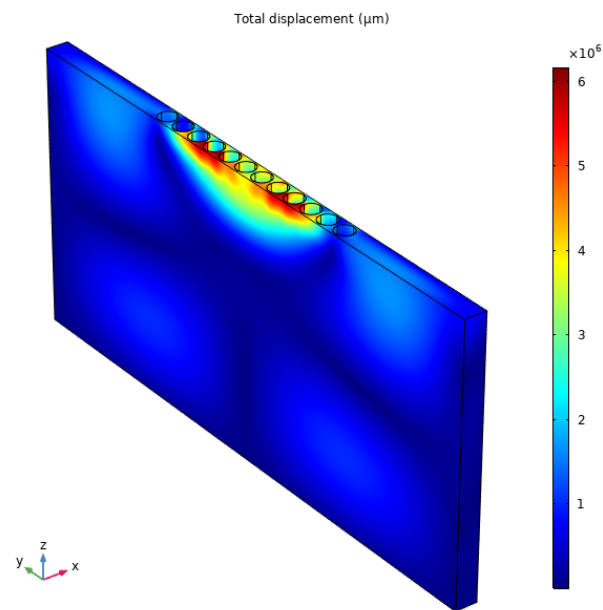


**Figure 14.** The magnitude of the total displacement field from the mode for the twelve-inclusion waveguide consisting of twelve 3  $\mu\text{m}$  deep inclusions. The eigenfrequency that was determined and displayed is 170.02 MHz.

1. Eigenfrequency Analysis. <https://www.comsol.com/multiphysics/eigenfrequency-analysis>, 2018. Accessed: October, 2023.
2. Muzar, E.; Stotz, J.A.H. Surface acoustic wave modes in two-dimensional shallow void inclusion phononic crystals on GaAs. *Journal of Applied Physics* **2019**, *126*, 025104. <https://doi.org/10.1063/1.5056311>.